

Simulation of the present-day climate with the climate model INMCM5

E. M. Volodin^{1,2}  · E. V. Mortikov^{1,2} · S. V. Kostykin¹ · V. Ya. Galin¹ · V. N. Lykossov^{1,2} · A. S. Gritsun¹ · N. A. Diansky¹ · A. V. Gusev¹ · N. G. Iakovlev¹

Received: 30 June 2016 / Accepted: 14 January 2017
© Springer-Verlag Berlin Heidelberg 2017

Abstract In this paper we present the fifth generation of the INMCM climate model that is being developed at the Institute of Numerical Mathematics of the Russian Academy of Sciences (INMCM5). The most important changes with respect to the previous version (INMCM4) were made in the atmospheric component of the model. Its vertical resolution was increased to resolve the upper stratosphere and the lower mesosphere. A more sophisticated parameterization of condensation and cloudiness formation was introduced as well. An aerosol module was incorporated into the model. The upgraded oceanic component has a modified dynamical core optimized for better implementation on parallel computers and has two times higher resolution in both horizontal directions. Analysis of the present-day climatology of the INMCM5 (based on the data of historical run for 1979–2005) shows moderate improvements in reproduction of basic circulation characteristics with respect to the previous version. Biases in the near-surface temperature and precipitation are slightly reduced compared with INMCM4 as well as biases in oceanic temperature, salinity and sea surface height. The most notable improvement over INMCM4 is the capability of the new model to reproduce the equatorial stratospheric quasi-biannual oscillation and statistics of sudden stratospheric warmings.

Keywords Climate · Model · Atmosphere · Ocean · Parameterization · Simulation · Temperature · Precipitation · Bias

✉ E. M. Volodin
volodinev@gmail.com

¹ Institute of Numerical Mathematic, Gubkina 8,
Moscow 119333, Russia

² Moscow State University, Leninskie Gory 1, Moscow, Russia

1 Introduction

This paper is devoted to the new version of the INMCM climate model that is being developed at the Institute of Numerical Mathematics of the Russian Academy of Sciences. This version (INMCM5) is an evolutionary upgrade of the previous version INMCM4, which was part of the CMIP5 (Coupled Model Intercomparison Project, Phase 5, Taylor et al. 2012). With the new version we are trying to reduce systematic model biases indicated in several papers devoted to the analysis of CMIP5 data and improve reproduction of some key processes responsible for the seasonal and interannual predictability.

The paper is structured as follows. First, we briefly describe the main features of the INMCM4's atmospheric and oceanic components as well as correspondent changes made in the INMCM5 [a detailed description of INMCM4 can be found in Volodin et al. (2010)]. Key improvements include the increase of the vertical resolution in the atmospheric module, revision of the large-scale condensation and cloud formation parameterizations, and the newly developed aerosol block. In the block of the ocean dynamics, the integration scheme for advection was changed (from coordinates splitting to an explicit one) and an iterative method for solving linear shallow water equation systems replaced the direct method used in INMCM4 (these changes were necessary to improve model scalability on parallel computers). In addition, the horizontal resolution of the oceanic model was doubled. The INMCM5 program code was reworked for better performance on parallel computers with distributed memory.

The second half of the paper describes the INMCM5 biases in the reproduction of the present-day climate with respect to the INMCM4 climate characteristics [Volodin

et al. (2010, 2013), Volodin (2013)] and that of the other CMIP5 models.

2 Model description

The family of INMCM climate models, as most climate system models, consists of two main blocks: the atmosphere general circulation model, and the ocean general circulation model. The atmospheric part is based on the standard set of hydrothermodynamic equations with hydrostatic approximation written in advective form. The model prognostic variables are wind horizontal components, temperature, specific humidity and surface pressure. The second order finite difference approximation uses the Arakawa C-grid (the spatial coordinates are geographical latitude, longitude and vertical sigma-coordinate). The leapfrog scheme with Asselin (1972) filtering is used for time stepping. The gravity waves are treated by implicit time scheme to improve numerical stability. Near the poles, the Fourier filter is applied along longitudinal direction to avoid numerical instability. Detailed description of the model's finite difference schemes as well as the set of the equations could be found in Alekseev et al. (1998) and Galin et al. (2003). The model version INMCM5 has a spatial resolution of $2 \times 1.5^\circ$ in longitude and latitude, and 73 levels in vertical. Lowermost and uppermost levels are placed at $\sigma = 0.993$ and $\sigma = 0.0002$, respectively. In the stratosphere, the model's vertical resolution is about 500 m [this resolution is important for correct description of interactions between the gravity wave drag parameterization and large scale flow to reproduce the Equatorial quasi-biannual oscillation (QBO)]. The time step in the dynamical block is 5 min for this particular spatial resolution. Previous model version (INMCM4) had similar atmospheric dynamical core, but with the uppermost level located at $\sigma = 0.01$ and with 21 vertical levels.

The INMCM5 borrows most of the atmospheric parameterizations from its previous version. One of the few notable changes is the new parameterization of clouds and large-scale condensation. In the INMCM5 cloud area and cloud water are computed prognostically according to Tiedtke (1993). That includes the formation of large-scale cloudiness as well as the formation of clouds in the atmospheric boundary layer and clouds of deep convection. Decrease of cloudiness due to mixing with unsaturated environment and precipitation formation are also taken into account. Evaporation of precipitation is implemented according to Kessler (1969). The INMCM4 in turn, determined cloud amount diagnostically. Similarly, cloud water is a diagnostically calculated function of temperature and pressure. Large scale condensation is obtained assuming that all specific

humidity exceeding the saturation threshold value instantly falls as precipitation [see Alekseev et al. (1998) for details].

Other atmospheric parameterizations in the INMCM5 are identical to the ones in the INMCM4 (some coefficients were re-adjusted to account for the changes in the vertical resolution). Deep and shallow convection parameterizations are analogous to Betts (1986), but with an additional mixing of momentum and with the penetration of deep convection a little higher than the level of zero buoyancy. Orographical and nonorographical gravity wave drags are implemented according to Palmer et al. (1986) and Hines (1997). In addition, nonorographical wave drag parameterization include vertical diffusion induced by the breaking of gravity waves.

The land surface and soil are represented according to Volodin and Lykossov (1998). Prognostic equations for soil temperature and soil specific humidity are solved at 23 levels from the surface to 10 m of depth, including freezing/melting of soil water. Spatial distribution of potential vegetation is prescribed, and actual vegetation is calculated using soil moisture in root zone. Maximum leaf area index for each vegetation type is prescribed, and actual leaf area index is determined using soil moisture and soil temperature.

Atmospheric radiation is calculated the same way as in Galin (1998). Solar spectrum is divided by four intervals and we use ten intervals to approximate the longwave part of the spectrum.

In the atmospheric boundary layer, vertical diffusion is applied to the prognostic variables (Alekseev et al. 1998). Entrainment of potential temperature, specific humidity, cloud area and cloud water at the top of the boundary layer are considered as in Tiedtke (1993). Calculation of cloud formation and condensation occurs at each time step of atmospheric dynamics. Atmospheric radiation is calculated once per 3 h, while the other atmospheric parameterizations are called every hour.

In the INMCM5 the atmospheric model is complemented by the interactive aerosol block, which is absent in the INMCM4. Concentrations of coarse and fine sea salt, coarse and fine mineral dust, SO_2 , sulfate aerosol, hydrophilic and hydrophobic black and organic carbon are all calculated prognostically. Dynamic processes described by the aerosol model include prescribed and simulated aerosol sources, advection, gravitational falling, wet and dry deposition and removal by precipitation. The model also takes into account the direct and indirect aerosol radiation effect that is connected with cloud drop radius and cloud water life time. The detailed description of the aerosol block used in the INMCM5 can be found in Volodin and Kostyrykin (2016).

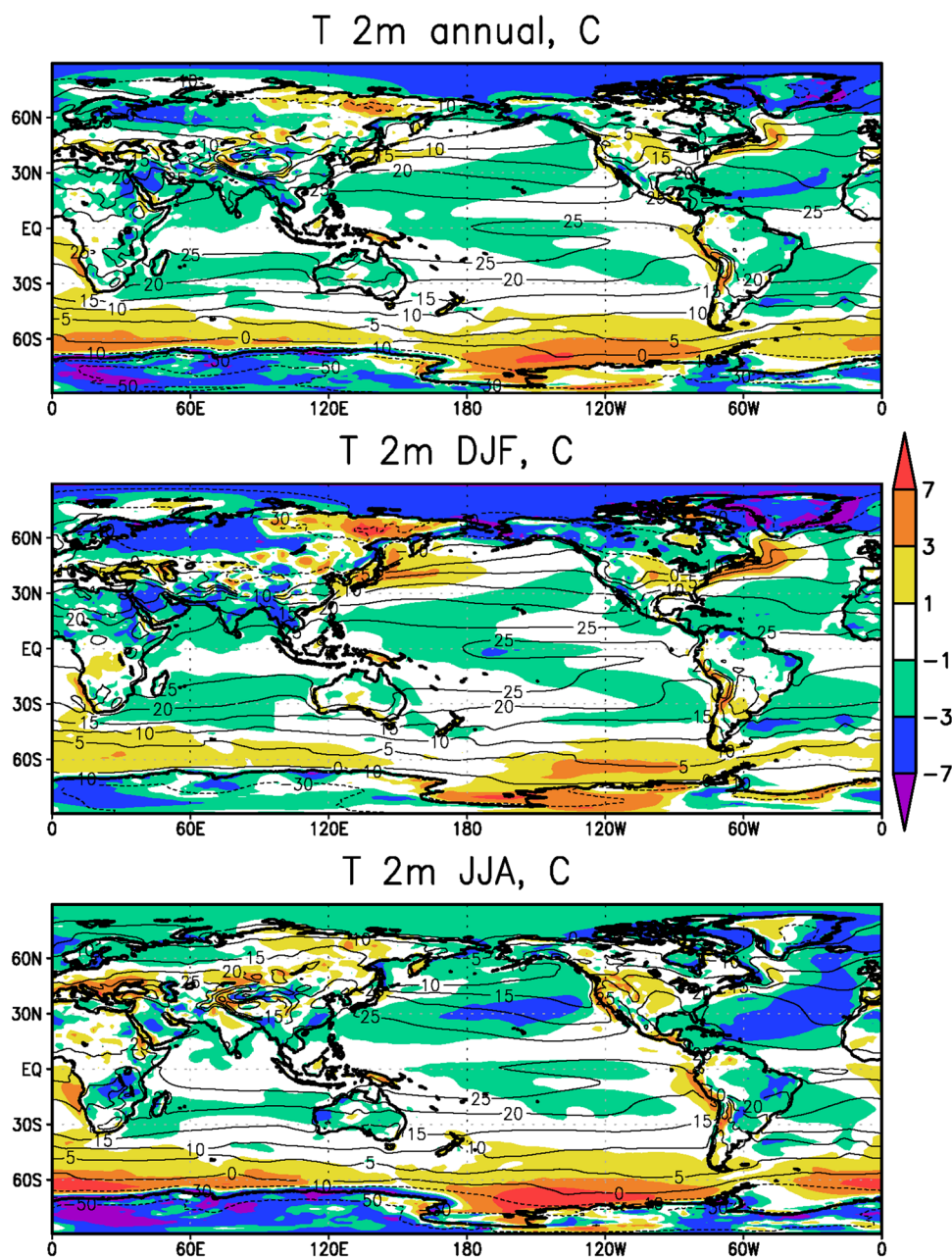
The oceanic module of the INMCM5 uses generalized spherical coordinates. The model "South Pole" coincides

with the geographical one, while the model “North Pole” is located in Siberia beyond the ocean area to avoid numerical problems near the pole. Vertical sigma-coordinate is used. The finite-difference equations are written using the Arakawa C-grid. The differential and finite-difference equations, as well as methods of solving them can be found in Zalesny et al. (2010). The INMCM5 uses explicit schemes for advection, while the INMCM4 used schemes based on splitting upon coordinates. Also, the iterative method for solving linear shallow water equation systems is used in the INMCM5 rather than direct method used in the INMCM4. The two previous changes were made to improve model parallel scalability. The horizontal resolution of the ocean

part of the INMCM5 is $0.5 \times 0.25^\circ$ in longitude and latitude (compared to the INMCM4's $1 \times 0.5^\circ$). Both the INMCM4 and the INMCM5 have 40 levels in vertical. The parallel implementation of the ocean model can be found in (Terekhov et al. 2011). The oceanic block includes vertical mixing and isopycnal diffusion parameterizations (Zalesny et al. 2010). Sea ice dynamics and thermodynamics are parameterized according to Iakovlev (2009). Assumptions of elastic-viscous-plastic rheology and single ice thickness gradation are used. The time step in the oceanic block of the INMCM5 is 15 min.

The climate model INMCM5 has a carbon cycle module (Volodin 2007), where atmospheric CO_2 concentration,

Fig. 1 Near-surface air temperature for annual (*top*), December–February (*middle*) and June–August (*bottom*) means. *Shading* (C) represents model bias with respect to ERA-Interim reanalysis data while isolines (at $-50, -30, -10, 0, 5, 10, 15, 20$ and 25 C) show model climatology. The 1979–2005 data interval was used to calculate averages



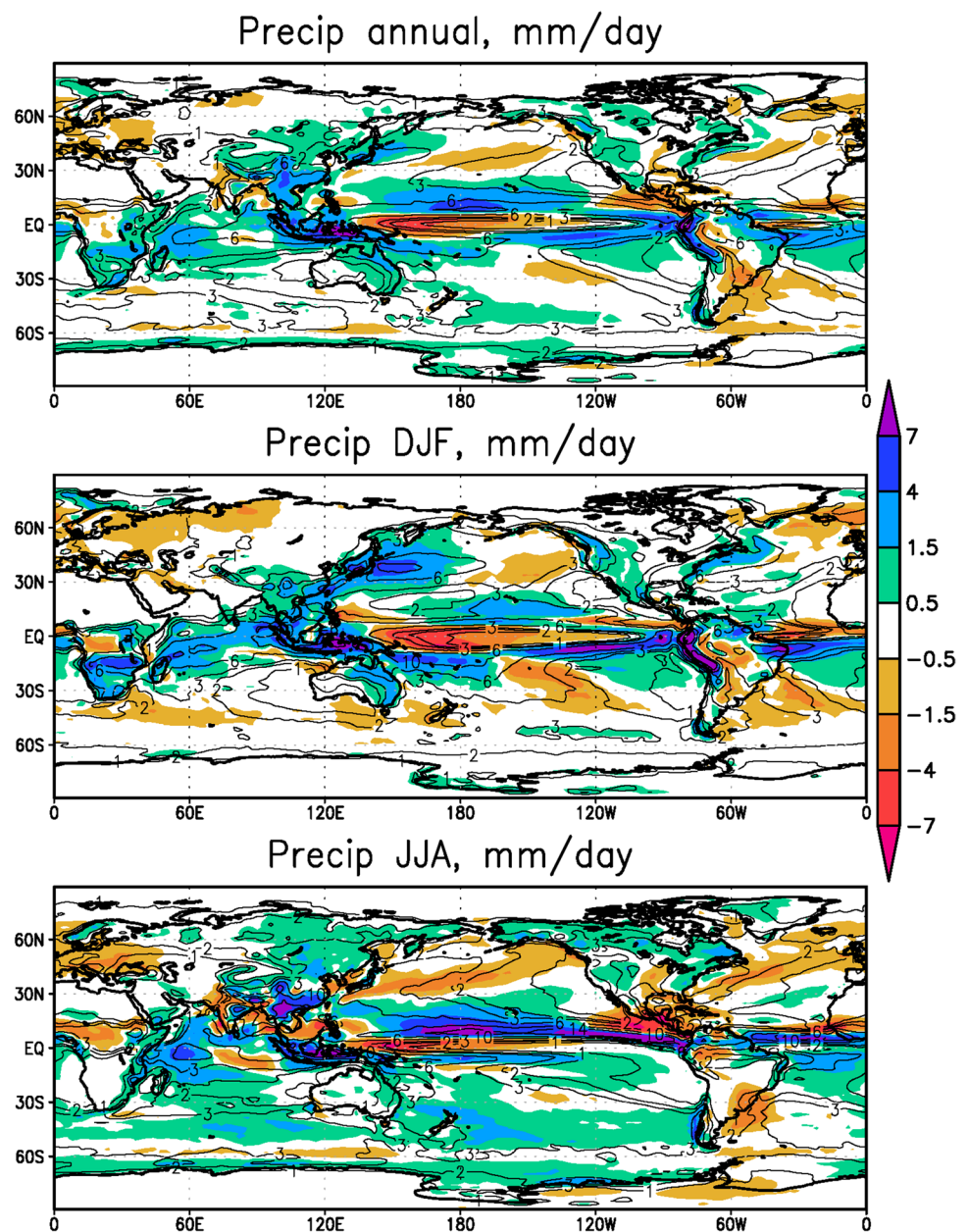
carbon in vegetation, soil and ocean are calculated. In soil, a single carbon pool is considered. In the ocean, the only prognostic variable in the carbon cycle is total inorganic carbon. Biological pump is prescribed. The model calculates methane emission from wetlands and has a simplified methane cycle (Volodin 2008). Parameterizations of some electrical phenomena, including calculation of ionospheric potential and flash intensity (Mareev and Volodin 2014), are also included in the model.

The codes of the atmospheric block, aerosol block and oceanic block are adopted for parallel computers by two-dimensional decomposition. The program's realization of the climate model allows for distributing calculations of

atmospheric dynamics, atmospheric aerosol and oceanic dynamics on different groups of processors using the MPI (Message Passing Interface) library. This possibility is also provided for the advection of oceanic tracers. The sea ice module is included in the oceanic block. The soil, surface and vegetation modules are included in the atmospheric block. The atmospheric and oceanic blocks exchange data once per 2 h. The atmospheric dynamics data are sent to the aerosol block at each dynamical time step. The aerosol concentration data are sent to the atmospheric block once per 3 h.

To reduce the number of synchronization points, the exchanges between the atmosphere and aerosol blocks

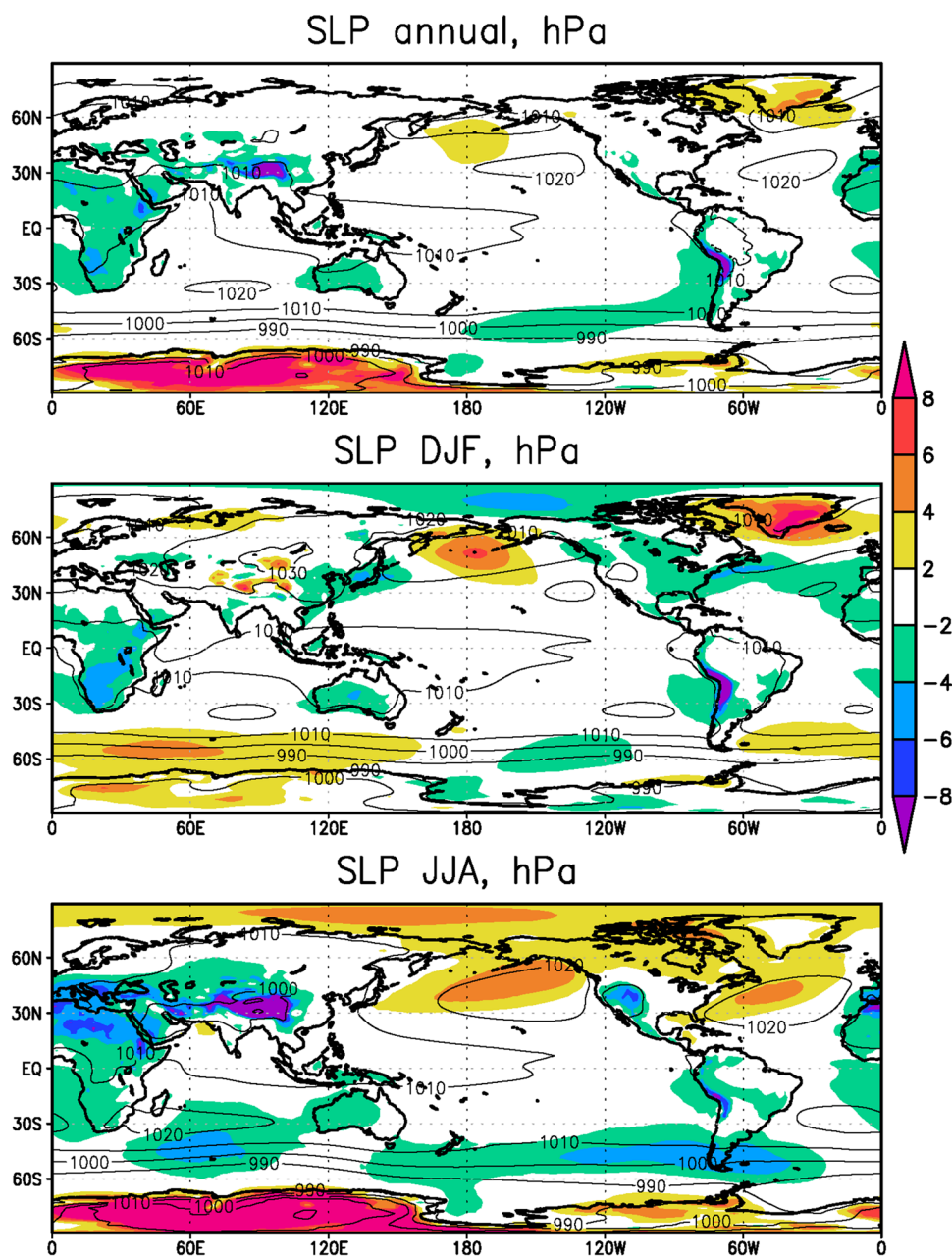
Fig. 2 Precipitation (mm day⁻¹) for annual (*top*), December–February (*middle*) and June–August (*bottom*) means. Shading represents model bias with respect to GPCP 2.2 data, while isolines (at 1, 2, 3, 6, 10 and 14 mm day⁻¹) show model climatology. The 1979–2005 data interval was used to calculate averages



are carried out asynchronously with additional buffering of messages. Numerical tests show that for the current model version, which has 10 prognostic variables in the aerosol block, an equal number of processors for atmospheric dynamics and aerosol block is optimal (giving acceleration by the factor of 2). For the INMCM5 the optimum number of cores at the supercomputer Lomonosov located in the Moscow State University is 96 for the atmospheric block, 96 for the aerosol block and 192 for the oceanic block (384 cores in total). Model performance in this case is about 6 model years per day.

Several INMCM5 model versions exist and share similar dynamical cores, parameterizations and parallel architecture, but have different spatial resolutions. The aim is to simulate the climate and climate changes at different time scales: from seasons to millennia. In addition to the basic model INMCM5 we have a model version for paleoclimate modeling (with a resolution of $5 \times 4^\circ$ and 21 levels in the atmosphere, and $2.5 \times 2^\circ$ and 40 levels in the ocean). The model INMCM5H with finer resolution ($0.67 \times 0.5^\circ$ and 73 levels in the atmosphere and $0.167 \times 0.125^\circ$ and 40 levels in the ocean) is capable of running for several decades and is aimed at HighResMIP experiments.

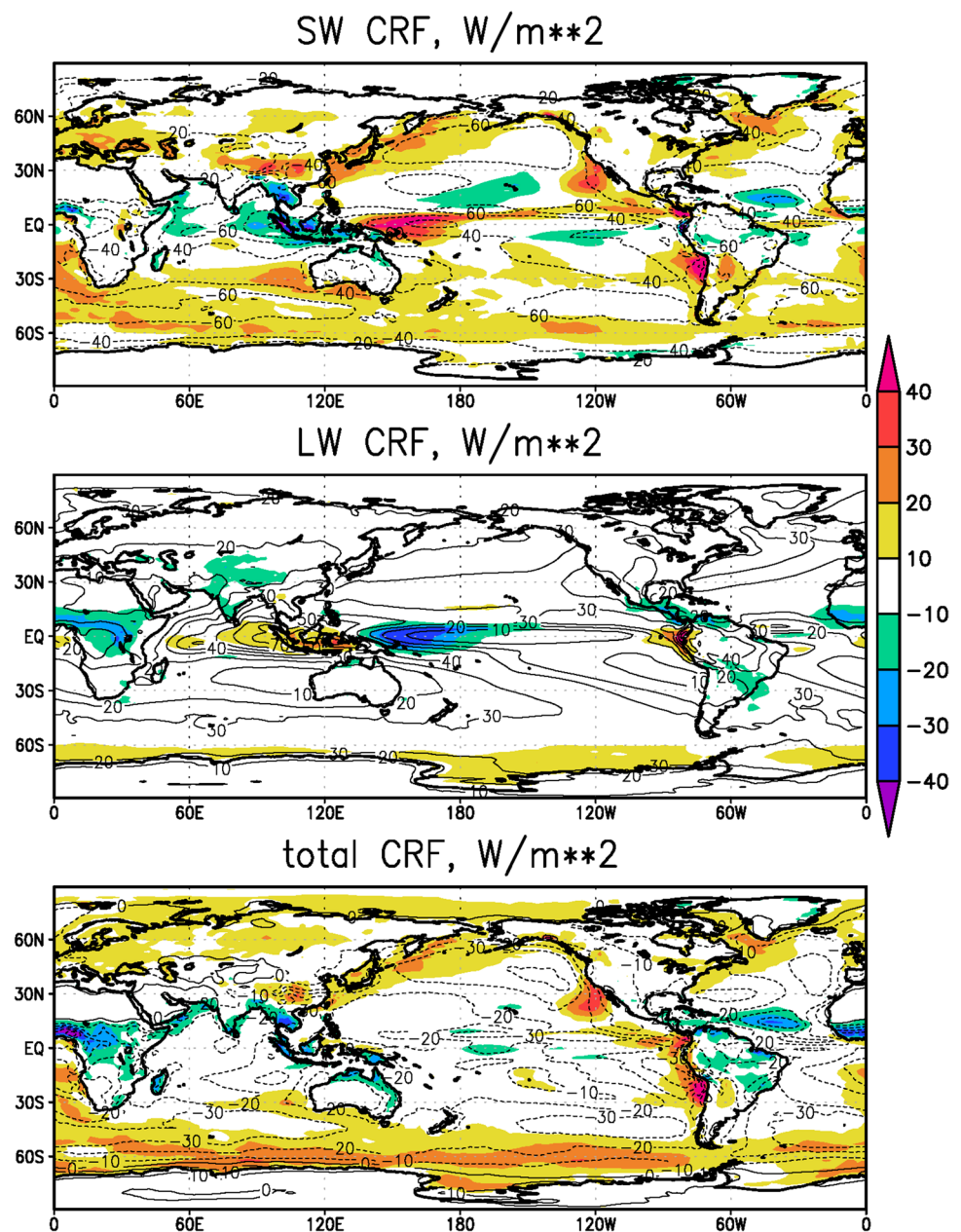
Fig. 3 Sea level pressure (hPa) for annual (*top*), December–February (*middle*) and June–August (*bottom*) means. Shading represents model bias with respect to the ERA-Interim reanalysis, while isolines (at 990, 1000, 1010 and 1020 hPa) show model climatology



3 Simulation of the present day climate

To estimate the quality of the new climate system and compare it with the previous one we performed a historical run for 1850–2005, where all forcings were specified according to the CMIP6 historical run protocol (<https://www.wcrp-climate.org/wgcm-cmip/wgcm-cmip6>). The initial conditions were taken from the model preindustrial run (where all the forcings were prescribed at the year 1850 conditions) after 300 years of integration. We mostly analyzed averages (seasonal or annual) over years 1979–2005 and restricted our attention to consideration of some basic features of atmospheric and oceanic dynamics and thermodynamics.

Fig. 4 Shortwave (*top*), long-wave (*middle*) and net (*bottom*) annual mean cloud radiative forcing (Wm^{-2}). Shading represents model bias with respect to the CERES v2.8 for 2000–2005, while isolines (from -60 to 40 Wm^{-2}) show model climatology



3.1 Atmosphere

Figure 1 presents the INMCM5 model bias in the near surface temperature with respect to the ERA-Interim (Dee et al. 2011) for annual, December–February and June–August means for 1979–2005. For the annual mean conditions, one can see cold bias over Arctic with the maximum in Greenland Sea and cold bias over Antarctica. Possible source of these errors is, probably, an insufficient amount of cloud ice in upper polar cloudiness. Positive temperature bias over the Southern ocean near Antarctica (mostly evident in the summer) can be attributed to underestimation of cloud radiation forcing (CRF) and

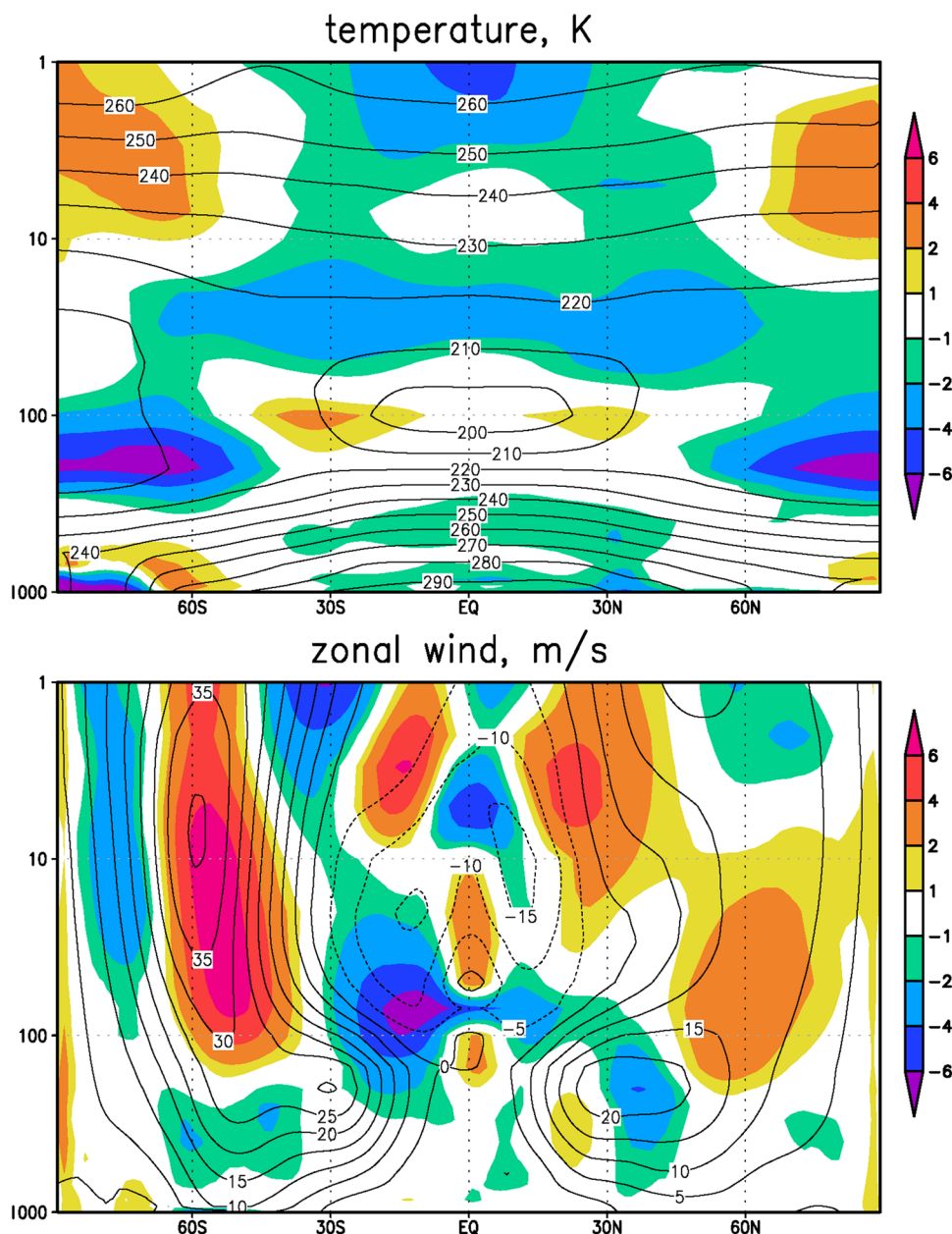
underestimation of sea ice compactness in the regions covered by ice.

When compared to the INMCM4 surface temperature climatology, the INMCM5 shows several improvements. Negative bias over continents is reduced mainly because of the increase in daily minimum temperature over land, which is achieved by tuning the surface flux parameterization. In addition, positive bias over southern Europe and eastern USA in summer typical for many climate models (Mueller and Seneviratne 2014) is almost absent in the INMCM5. A possible reason for this bias in many models is the shortage of soil water and suppressed evaporation leading to overestimation of the surface temperature. In

the INMCM5 this problem was addressed by the increase of the minimum leaf resistance for some vegetation types. Nevertheless, some problems migrate from one model version to the other: negative bias over most of the subtropical and tropical oceans, and positive bias over the Atlantic to the east of the USA and Canada. Root mean square (RMS) error of annual mean near surface temperature was reduced from 2.48 K in the INMCM4 to 1.85 K in the INMCM5.

Model bias in precipitation with respect to GPCP v.2.2 (Adler et al. 2003) can be seen in Fig. 2. Over the tropics, one can see the typical precipitation error for contemporary climate models: overestimation of precipitation in the western Indian Ocean, Indonesia, Atlantic Ocean south of

Fig. 5 Annual mean zonal mean air temperature (K, top) and zonal mean zonal wind (ms^{-1} , bottom). Shading represents model bias with respect to the ERA-Interim data for 1979–2005, isolines show model climatology

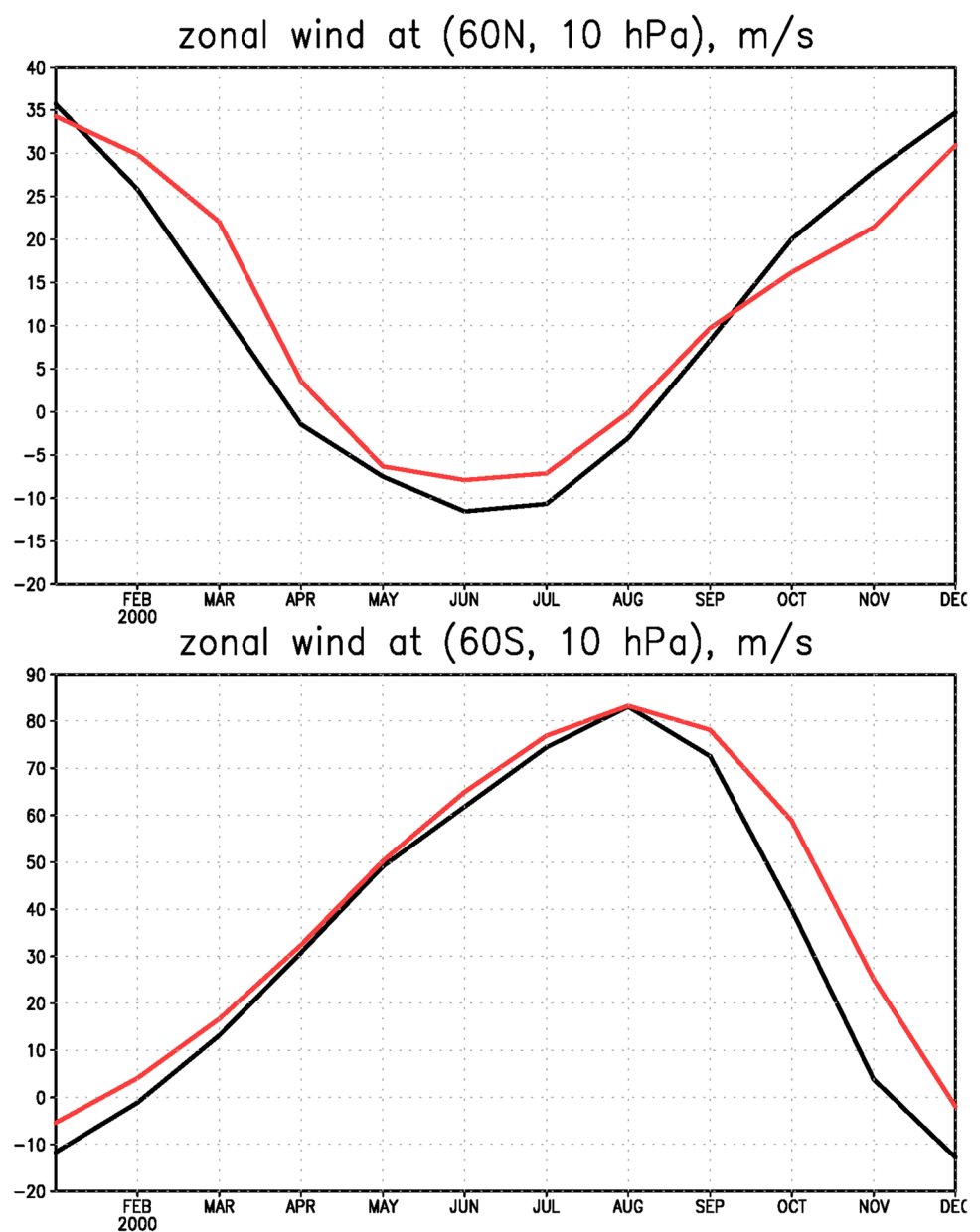


the Equator, and in the tropical Pacific outside of Equator. Model precipitation is underestimated over the equatorial Pacific, Central America and Brazil. All the listed shortcomings are seen in the figure representing model bias averaged over all the CMIP5 models (Flato et al. 2013, Fig. 9.4). In midlatitudes, the positive precipitation bias over the ocean prevails in winter while negative bias occurs in summer. Compared to the INMCM4, the biases over the western Indian Ocean, Indonesia, the eastern tropical Pacific and the tropical Atlantic are reduced. A possible reason for this is the better reproduction of the tropical sea surface temperature (SST) in the INMCM5 due to the increase of the spatial resolution in the oceanic block, as well as the new condensation scheme. RMS annual

mean model bias for precipitation is 1.35 mm day^{-1} for the INMCM5 compared to 1.60 mm day^{-1} for the INMCM4.

Figure 3 presents model bias in sea level pressure (SLP) with respect to the 1979–2005 ERA-Interim data. The model underestimates annual mean SLP over most parts of Africa and southern Eurasia, and overestimates it in the North Pacific and Atlantic sector of the Arctic. These shortcomings do not change significantly from season to season. In the southern midlatitudes, positive bias in summer tends to compensate for negative bias in winter. Large SLP bias in the Antarctic in Austral winter could be attributed to the discrepancy between model and ERA-Interim reanalysis methods for calculation of SLP in regions with high elevation. Large bias in the Tibet has probably the same origin.

Fig. 6 Annual cycle of zonal mean zonal wind (m s^{-1}) at 10 hPa, 60N (top) and 60S (bottom). Red line model data, black line ERA Interim data. The 1979–2005 period was used for calculation of averages

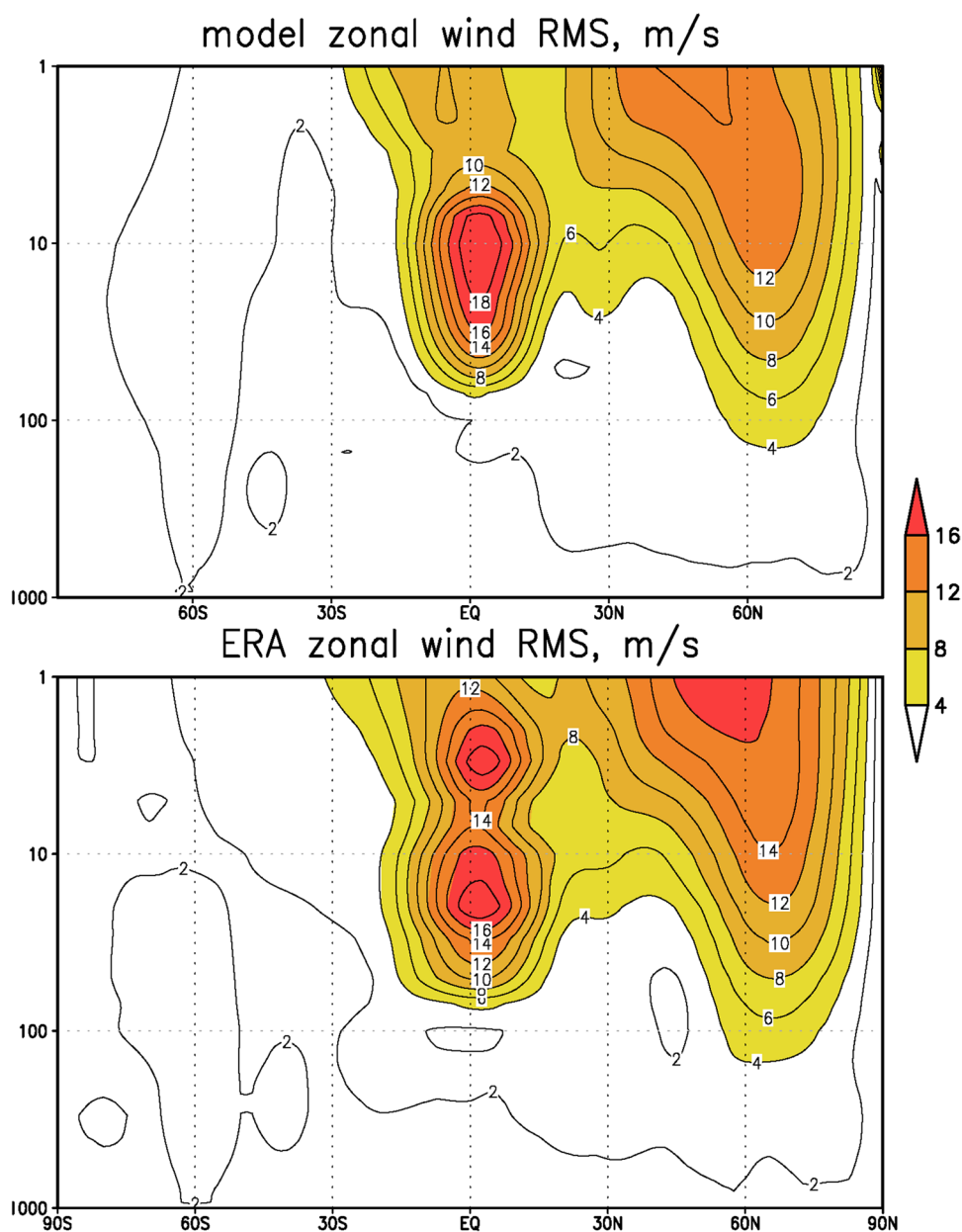


The RMS bias of annual mean SLP is equal to 1.86 hPa for the INMCM5, while it is 2.15 hPa for INMCM4.

Cloud radiation forcing (CRF) at the top of the atmosphere is one of the most important climate model characteristics, as errors in CRF frequently lead to an incorrect surface temperature. Annual mean shortwave, longwave and net CRF for the model and CERES v.2.8 (Loeb et al. 2009) are shown in Fig. 4 (time mean over 2000–2005 is used for model and CERES data). The model underestimates the absolute value of shortwave forcing in the subtropics and midlatitudes by approximately $10\text{--}20\text{ W m}^{-2}$. In the subtropical regions of marine stratocumulus model error is even higher. Total shortwave forcing in the tropics is not far from the observed one, but one can see regional errors due

to the model shift of the intertropical convergence zone. In the high latitudes model errors in shortwave CRF are small. The model underestimates longwave CRF in the subtropics but overestimates it in the high latitudes. Errors in longwave CRF in the tropics tend to partially compensate errors in shortwave CRF. Both errors have positive sign near 60S leading to warm bias in the surface temperature here. As a result, we have some underestimation of the net CRF absolute value at almost all latitudes except the tropics. Additional experiments with tuned conversion of cloud water (ice) to precipitation (for upper cloudiness) showed that model bias in the net CRF could be reduced, but that the RMS bias for the surface temperature will increase in this case.

Fig. 7 RMS of monthly mean zonal mean zonal wind, ms^{-1} , in December–February in the model (*top*) and ERA-Interim (*bottom*)



The model zonal and annual mean temperature (Fig. 5) exhibits 4–6 K negative bias near the polar tropopause, which is usual for many climate models. Positive bias near the tropical tropopause is about 1–2 K. It is smaller than the one in the INMCM4, where the positive bias was equal to 4–5 K. The reason for this improvement is the adjustment of the deep convection parameterization. In the troposphere, the magnitude of the temperature bias is about or below 2°, except mountain areas where temperature extrapolation at low pressure levels is required. The model bias for zonal and annual mean zonal wind is about or less than 4 m s⁻¹ in the troposphere and never exceeds 8 m s⁻¹ in the stratosphere, which seems satisfactory. Analysis of the annual cycle of zonal wind at 10 hPa and 60N (Fig. 6) shows that model tends to overestimate zonal wind by 5–10 m/s in February–August and underestimate it in October–December, that leads to small annual mean error. In the Southern stratosphere at 60S positive model bias in zonal wind is mostly pronounced in October–December, when model wind is 10–15 m/s higher than in the reanalysis. The reason for this error is underestimated meridional heat flux induced by planetary waves propagating upward.

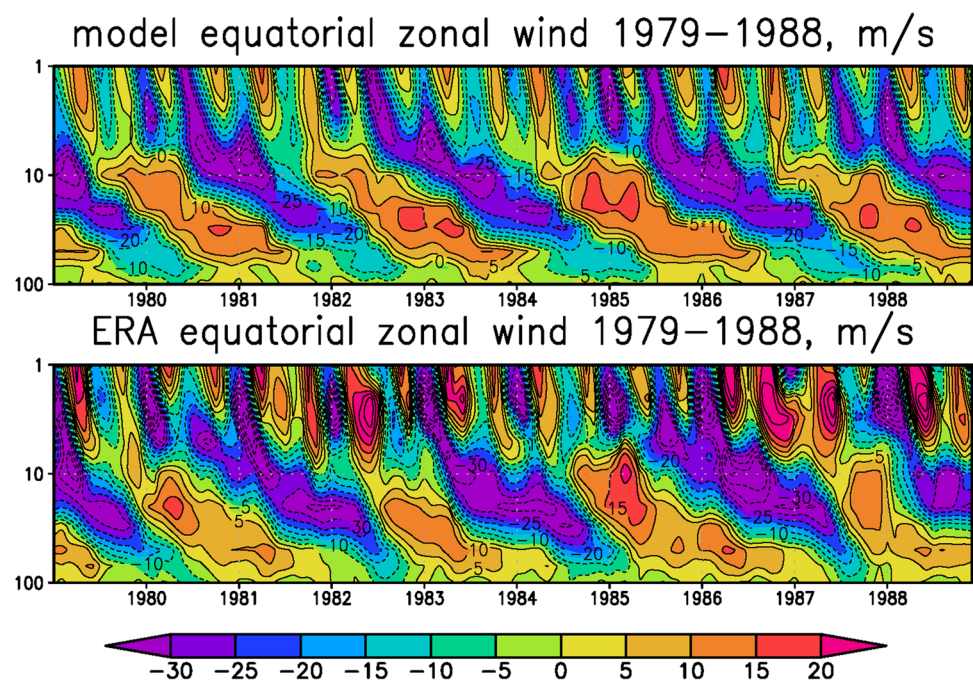
Several important features of the stratosphere dynamics could be described in terms of monthly mean zonal wind RMS (see Fig. 7). In the Northern Hemisphere the strongest variability of the wind takes place in December–February so the RMS for the winter season is shown. The RMS maximum near the Equator is about 18 m s⁻¹ in the ERA-Interim, and about 18 m s⁻¹ in the model. This maximum is

a manifestation of the equatorial QBO. To consider model QBO in details, on Fig. 8 we represent time series of zonal equatorial wind in the stratosphere for years 1979–1988. The QBO amplitude in the model is not far from the observations. One can see downward propagation of the QBO signal from level of 5–100 hPa both in the model and ERA data. At levels of 1–5 hPa semiannual oscillation can be seen, some of them initiate phase change of the QBO. The QBO period is about 28 months in the observational data, and about 29–30 months in the model. The procedure for the adjustment of QBO amplitude and period by tuning parameters for nonorographic gravity wave drag, vertical and horizontal diffusion can be found in Kulyamin et al. (2009).

Interaction of zonal mean flow and long planetary waves induce high variance of zonal wind in winter in the stratosphere mid- and highlatitudes. Maximum RMS in the midlatitudes is about 14–16 m s⁻¹ in ERA-Interim data, and 12–14 m s⁻¹ in the model data (Fig. 7).

An important indicator of the winter stratospheric variability is the number of sudden stratospheric warmings (SSW). Here we define the SSW event as one when the zonal mean of zonal wind at 60N and 10 hPa is negative. In the model, we have about 20 SSWs per 30 years, while in the observations we have 18 SSWs per 30 years (Butchart et al. 2011). Figure 9 presents amplitudes of stationary waves in geopotential height in the model and ERA-Interim for the northern hemisphere winter. The amplitude of wave number 1 is underestimated in the model by 10–15%, while the amplitude of wave number

Fig. 8 Time series of zonal mean zonal wind (m s⁻¹) in the stratosphere at Equator for 1979–1988 in the model (*top*) and Era Interim (*bottom*)



2 in the model is close to the reanalysis data. In general, in the INMCM5 the winter stratospheric variability is reproduced reasonably well. The detailed study of

the INMCM5 stratospheric dynamics including analysis of the SSWs, its influence on the lower stratosphere and troposphere can be seen in Vargin and Volodin (2016).

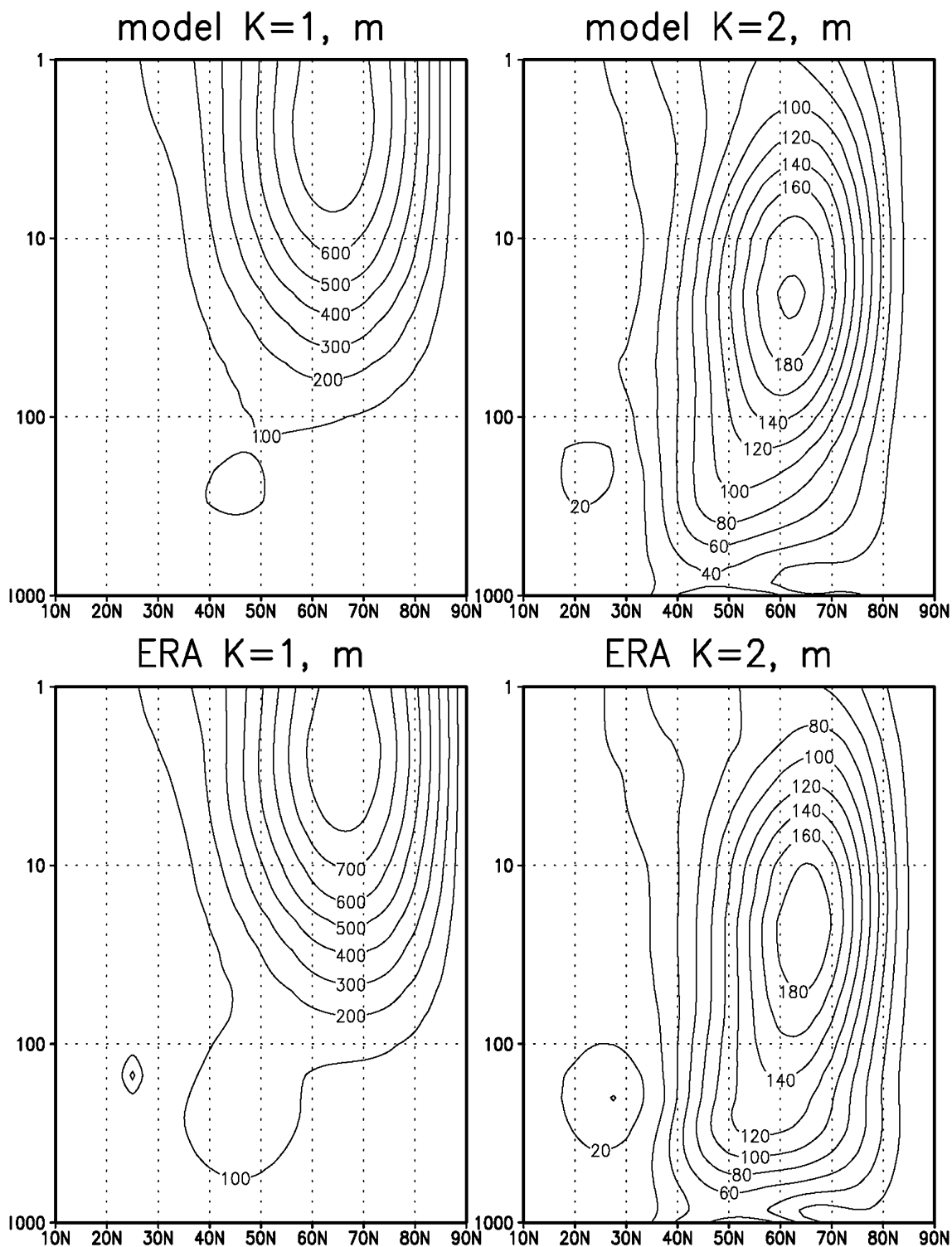


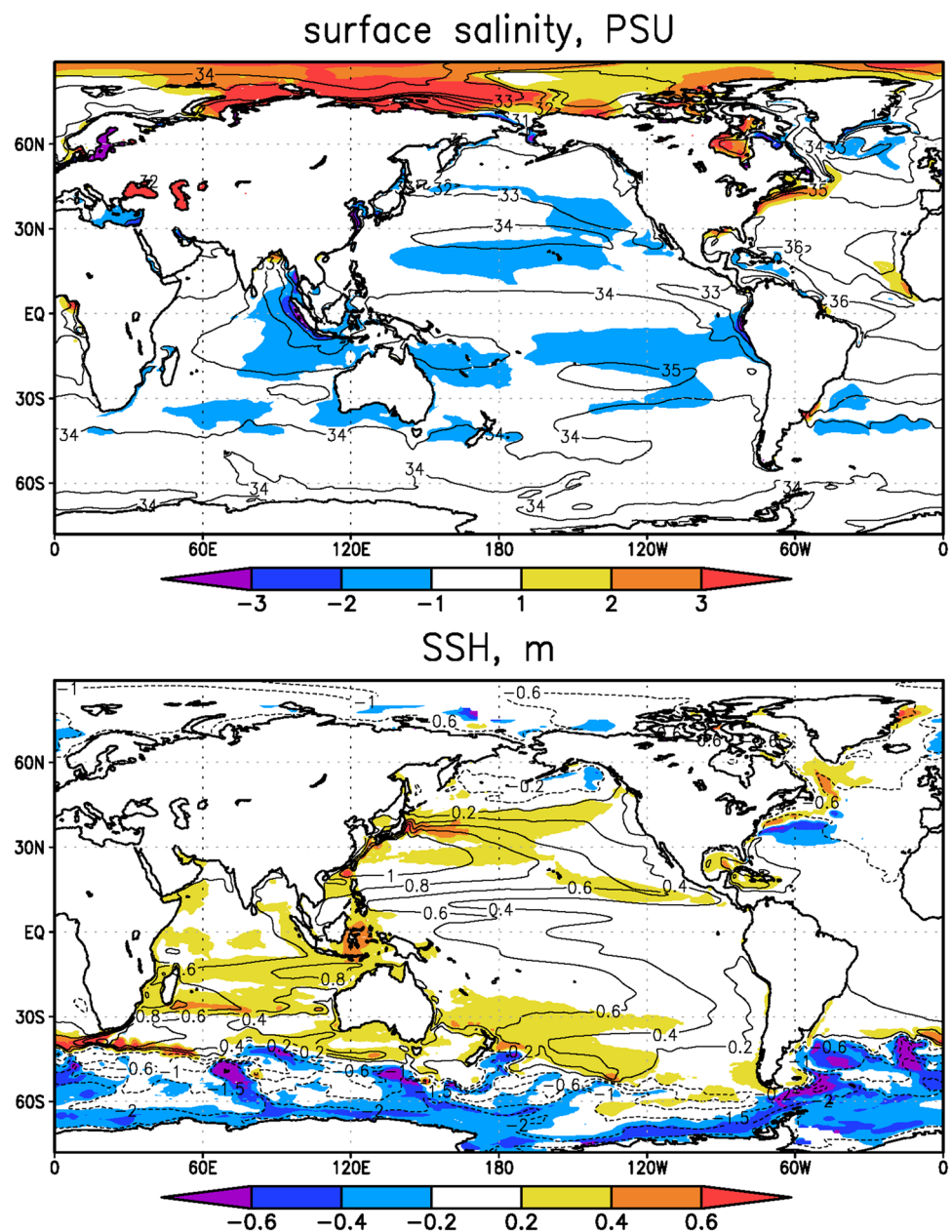
Fig. 9 Amplitude of the wave number 1 (left) and the wave number 2 (right) in geopotential height (m) in December–February in the model data (top) and ERA-Interim (bottom)

3.2 Ocean

Let us first consider the basic features of oceanic mean state. Figure 10 presents model bias in the surface salinity and the mean dynamical sea surface height with respect to the World Ocean Atlas 2009 (WOA09, Antonov et al. 2010) and Rio and Hernandez (2004). On average, the model produces negative bias in surface salinity, but it is not as high as in the INMCM4. A possible reason for this improvement is the increase in the oceanic model resolution by the factor of two in both horizontal directions and new representation of advection by large oceanic eddies. In the Arctic, the INMCM5 has a positive bias in salinity up to 1–5 PSU.

It seems that polar river runoff is underestimated in the model, and positive bias can be attributed to strong vertical mixing. RMS error of the surface salinity in the INMCM5 is much better than that in the INMCM4 (0.78 PSU compared to 1.20 PSU). A study by Landerer et al. (2014) shows large bias in sea surface height in the INMCM4 (RMS of the model bias is 0.36 m). In the INMCM5, RMS model bias is reduced to 0.19 m. Nevertheless, one can see some underestimation of sea surface height in the Southern Ocean and its overestimation by 0.1–0.3 m in the Indian Ocean and partially in the Pacific. These biases cannot be attributed to temperature bias because surface temperature and temperature in upper 700 m in the Southern Ocean (see

Fig. 10 Annual mean model bias in sea surface salinity (PSU) with respect to WOA09 (Antonov et al. 2010) data (*top*) and sea surface height (m) with respect to (Rio and Hernandez 2004) (*bottom*)



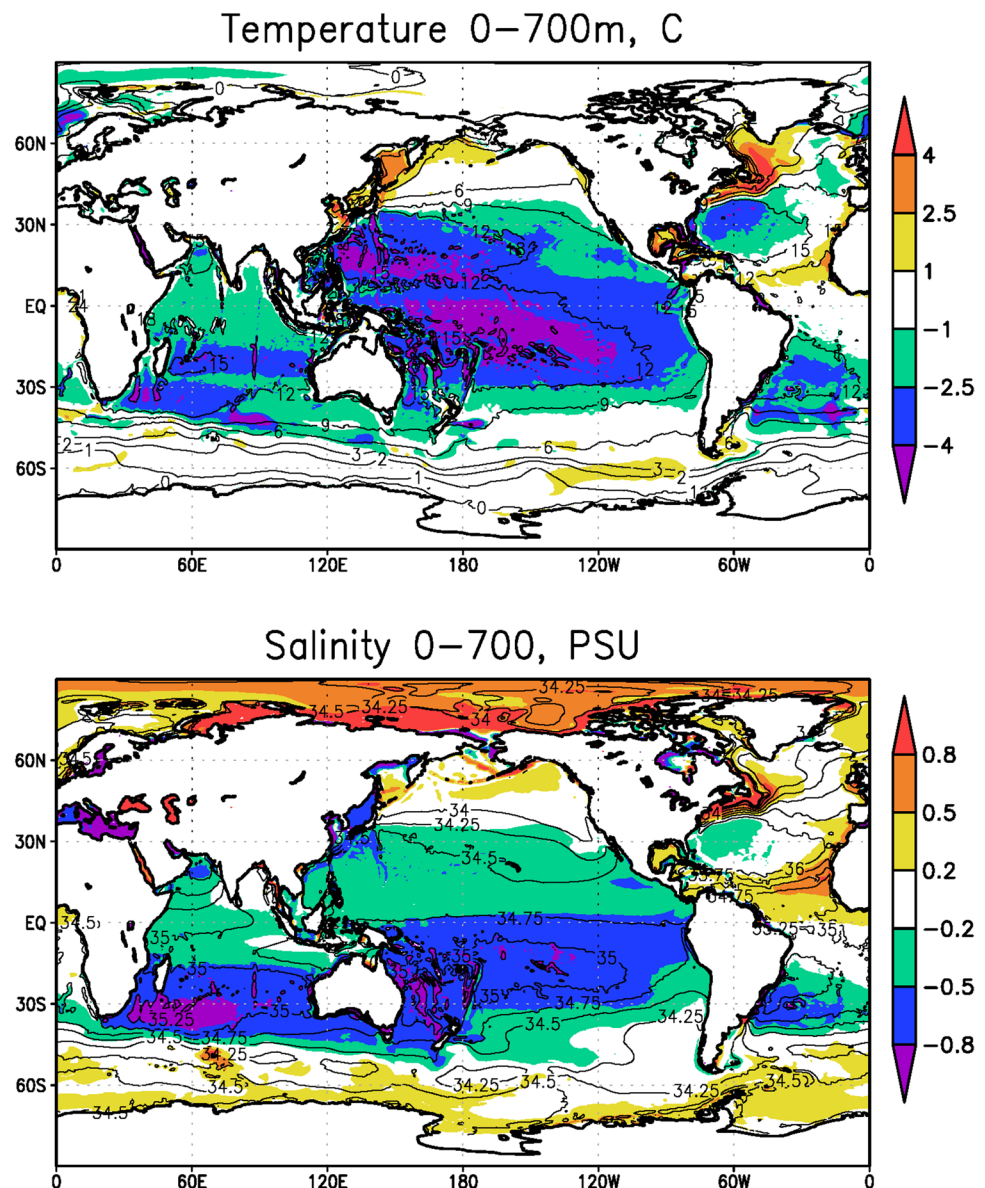
below) in the model are not far from the observed (with positive biases), while in the Indian Ocean they are lower than the observed ones. Further analysis of the sea surface height characteristics (including its natural variability) for different versions of the INM climate models with different spatial resolutions in the ocean can be found in Iakovlev et al. (2016).

The model annual mean temperature and salinity bias [with respect to WOA09 (Antonov et al. 2010)] in the upper 700 m layer are presented in Fig. 11. Generally, one can see cold bias in the tropical regions, and warm bias in the southern midlatitudes, the north-west Atlantic and the north-west Pacific. In the regions with positive temperature bias, salinity bias is also positive, and vice versa. The exception is the Arctic Ocean, where one can see positive

salinity and negative temperature errors. At least part of the temperature biases can be attributed to the shortcomings of the atmospheric model. Small values of CRF over the Southern ocean lead to a positive bias in the SST and temperature of the upper oceanic layers. We suppose that possible reason of positive bias in the Arctic salinity is a strong vertical mixing in the upper layer, but additional model runs are required to prove this hypothesis.

The model biases in potential temperature and salinity averaged over longitude with respect to WOA09 (Antonov et al. 2010) are shown in Fig. 12. Positive bias in the Southern Ocean penetrates from the surface downward for up to 300 m, while negative bias in the tropics can be seen even in the 100–1000 m layer. Nevertheless, zonal mean temperature error at any level from the surface to the bottom

Fig. 11 Annual mean model bias in mean temperature, C (top), and salinity, PSU (bottom), in the 0–700 m ocean layer with respect to WOA09 (Antonov et al. 2010). Shading represents bias, contours show observed state



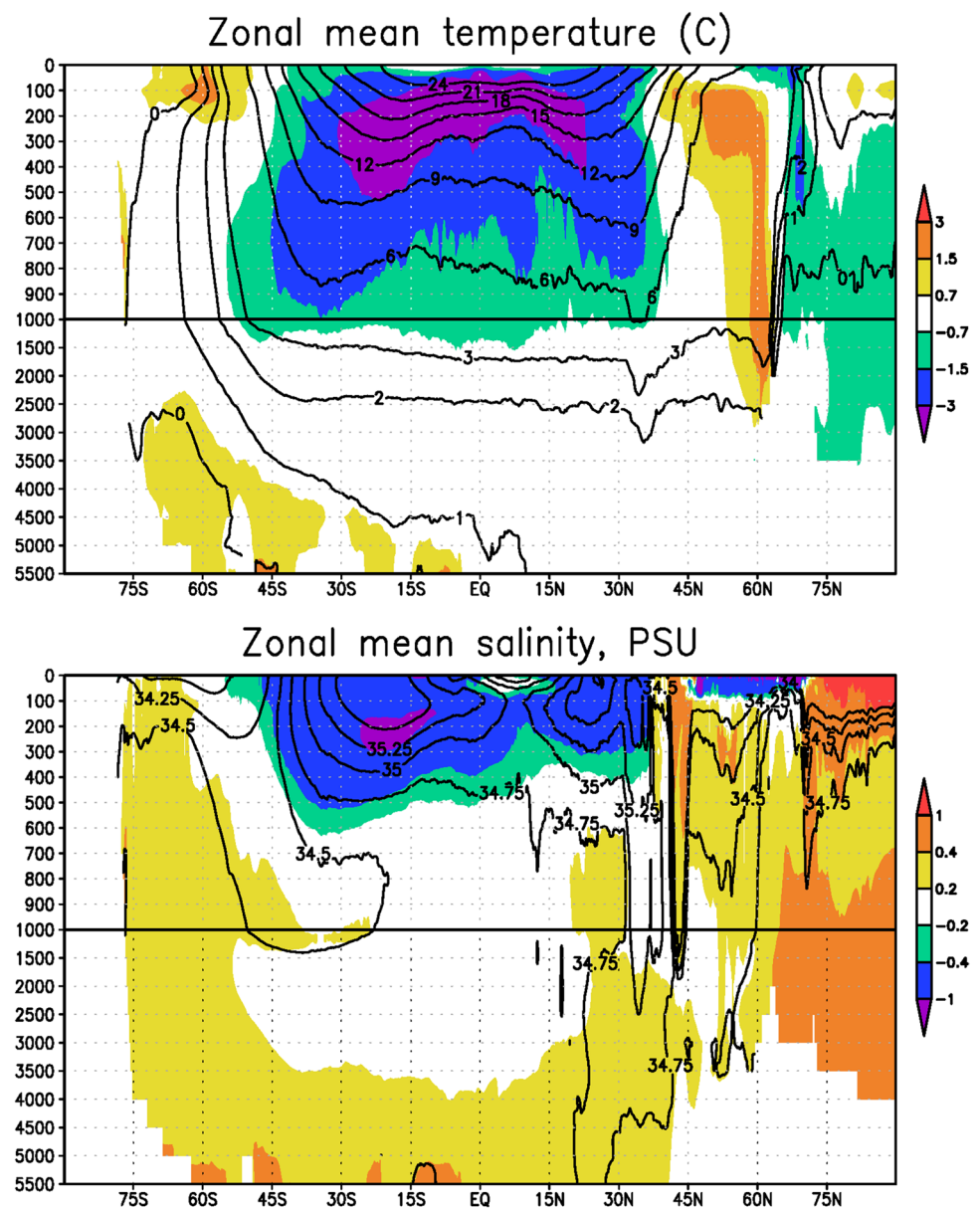
is small. This was not the case for the INMCM4, where one could see negative temperature bias up to 2–3 K from 1.5 km to the bottom nearly at all latitudes, and 2–3 K positive bias at levels of 700–1000 m. The reason for this improvement is the introduction of a higher background coefficient for vertical diffusion at high depth (3000 m and higher) than at intermediate depth (300–500 m). Positive temperature bias at 45–65 N at all depths could probably be explained by shortcomings in the representation of deep convection [similar errors can be seen for most of the CMIP5 models (Flato et al. 2013, their Fig. 9.13)]. Another feature common for many present day climate models (and for the INMCM5 as well) is negative bias in southern tropical ocean salinity from the surface to 500 m. It can be

explained by overestimation of precipitation at the southern branch of the Inter Tropical Convergence zone.

Meridional heat flux in the ocean (Fig. 13) is not far from available estimates (Trenberth and Caron 2001). It looks similar to the one for the INMCM4, but maximum of northward transport in the Atlantic in the INMCM5 is about $0.1\text{--}0.2 \times 10^{15}$ W higher than the one in the INMCM4, probably, because of the increased horizontal resolution in the oceanic block.

Sea ice area is an important parameter of the model cryosphere. Figure 14 shows the annual cycle of sea ice area in the Arctic and Antarctic. Data by Hurrell et al. (2008) for 1979–2005 were chosen as the observations. In the Arctic, the model sea ice area is just slightly overestimated.

Fig. 12 Zonal and annual mean model bias in potential temperature, C (*top*), and salinity, PSU (*bottom*), with respect to WOA09 (Antonov et al. 2010). Shading represents bias, contours represent observed state



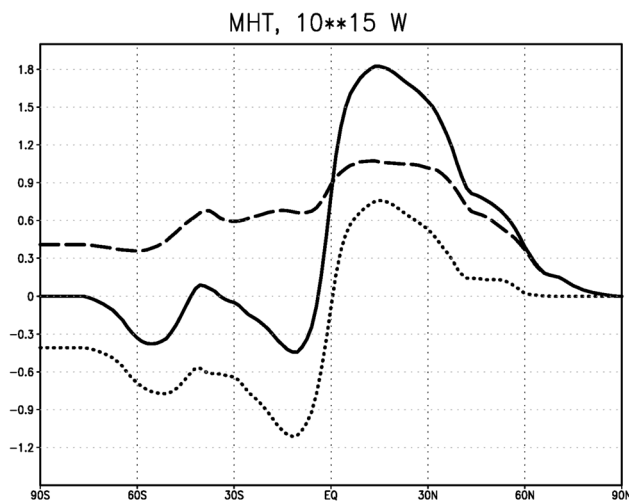


Fig. 13 Meridional heat transport, 10^{15} W, in the Global Ocean (solid line), Atlantic (dashed line) and Indo-Pacific (dotted line) in the model

Overestimation of the Arctic sea ice area is connected with negative bias in the surface temperature. In the same time, connection of the sea ice area error with the positive salinity bias is not evident because ice formation is almost compensated by ice melting, and the total salinity source for these pair of processes is not large. The amplitude and phase of the sea ice annual cycle are reproduced correctly by the model. In the Antarctic, sea ice area is underestimated by a factor of 1.5 in all seasons, apparently due to the positive temperature bias. Note that the correct simulation of sea ice area dynamics in both hemispheres simultaneously is a difficult task for climate modeling.

The El Niño is one of the most important phenomena of interannual variability in atmosphere and ocean. The RMS deviation for the monthly mean surface temperature in the tropical Pacific for the model and the ERSST v4 (Huang et al. 2015) data are shown in Fig. 15. RMS values in the model are underestimated by a factor of 1.2–1.5, but the location of variance maximum is reproduced correctly. In the INMCM4, the surface temperature variability was also underestimated but the El Niño tended to propagate too westward in the west Pacific while the RMS maximum near America was absent. The improvements could probably be attributed to the horizontal resolution increase in the oceanic model. However, the reason for the underestimated El Niño amplitude is unclear and requires further studies. The analysis of the model time series of the SST anomalies shows that the El Niño event frequency is approximately the same in the model and data, but the model El Niños happen too regularly. Atmospheric response to the El Niño

events is also underestimated in the model by a factor of 1.5 with respect to the reanalysis data. Time spectra of the model and observed SST (ERSST v4 data) in NINO3,4 region (Fig. 16) show that in the observations there is spectral peak at 50 months attributed to the El-Niño. In the model, two peaks associated with El-Niño can be seen at 50 and 80 months but they are weaker by the factor of 1.5–2 compared with the data.

3.3 Carbon cycle

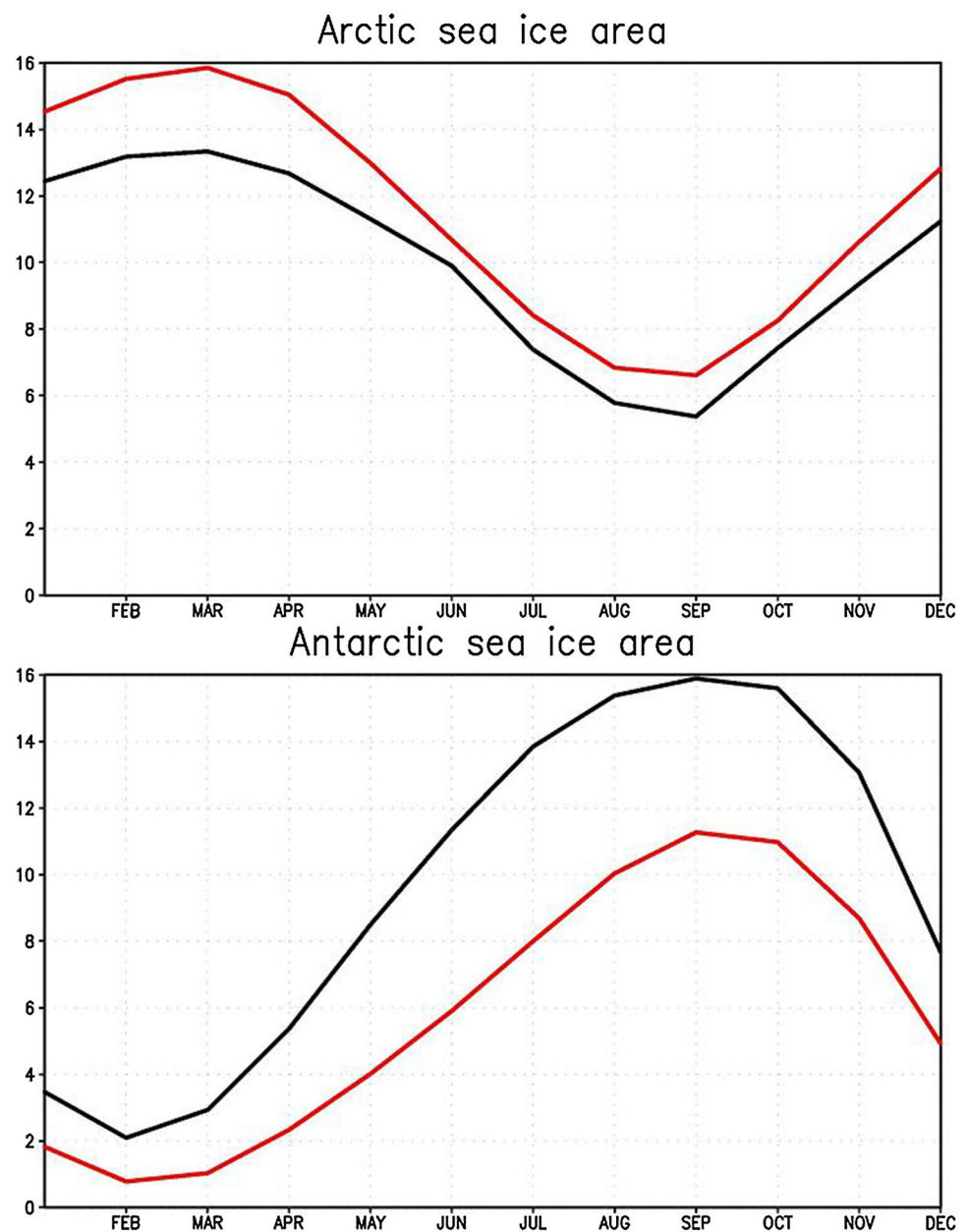
In this section we present some integral characteristics of model carbon cycle module. Gross primary production (GPP) of the land vegetation in the model for 1986–2005 is 155 GtC/yr, while GPP for CMIP5 models lies in the interval from 105 to 178 GtC/yr (Anav et al. 2013). Estimations of this value from the observations gives values from 114 GtC/yr (Mao et al. 2012) to 150–175 GtC/yr (Welp et al. 2011). Annual cycle of GPP for the global domain, the tropics, the northern and southern extratropics can be seen at Fig. 17. The estimate of observed annual cycle is given by Jung et al. (2009), where global mean value is 120 GtC/yr. One can see that model GPP is higher than that of Jung et al. (2009) in all subdomains however the seasonal cycle is reproduced reasonably well for all domains except the tropics. Note that the GPP seasonal cycle in the tropics is poorly reproduced by many CMIP5 models (see Fig. 9 in Anav et al. 2013).

Global vegetation carbon amount in the model for 1986–2005 is 629 GtC while it is 522 ± 162 GtC for CMIP5 models (Anav et al. 2013). Global soil carbon amount is 1781 GtC in the model and 1502 ± 798 GtC in CMIP5 models. Estimation of observed values of vegetation and soil carbon are 550 GtC and 1340 GtC (Todd-Brown et al. 2012).

Annual cycle of the net carbon flux from the atmosphere (to vegetation, soil and ocean) can be seen in Fig. 18. Estimation of observed values is from Jung et al. (2009). Model underestimates the amplitude of the annual cycle of net carbon flux in global domain and Northern extratropics by the factor of 1.5–2. Also, the maximum uptake in the model is 1 month earlier than in the Jung et al. (2009) data. Probable reason for this discrepancy is different behavior of plant and soil respiration in the model and reality. Similar large deviations from the observed data are also common for many CMIP5 models (see Fig. 7 in Anav et al. 2013).

In general, model reproduces basic features of carbon cycle reasonably well. Other details of the model carbon cycle including trend of carbon uptake in historical run will be a subject of specific paper.

Fig. 14 Annual cycle of sea ice area, 10^6 km^2 , in the Northern (*top*) and Southern (*bottom*) Hemisphere in the model (*red*) and Hurrell et al. (2008) (*black*) for 1979–2005



4 Conclusion

Based on the CMIP5 model INMCM4 the next version of the Institute of Numerical Mathematics RAS climate model was developed (INMCM5). The most important changes include new parameterizations of large scale condensation (cloud fraction and cloud water are now the prognostic variables), and increased vertical resolution in the atmosphere (73 vertical levels instead of 21, top model level raised from 30 to 60 km). In the oceanic block, horizontal resolution was increased by a factor of 2 in both directions.

The climate model was supplemented by the aerosol block. The model got a new parallel code with improved computational efficiency and scalability.

With the new version of climate model we performed a test model run (80 years) to simulate the present-day Earth climate. The model mean state was compared with the available datasets. The structures of the surface temperature and precipitation biases in the INMCM5 are typical for the present climate models. Nevertheless, the RMS error in surface temperature, precipitation as well as zonal mean temperature and zonal wind are reduced in the INMCM5

Fig. 15 RMS of monthly mean surface temperature (K) in tropical Pacific for ERSST v4 (Huang et al. 2015) data (top) and model (bottom) for 1979–2005

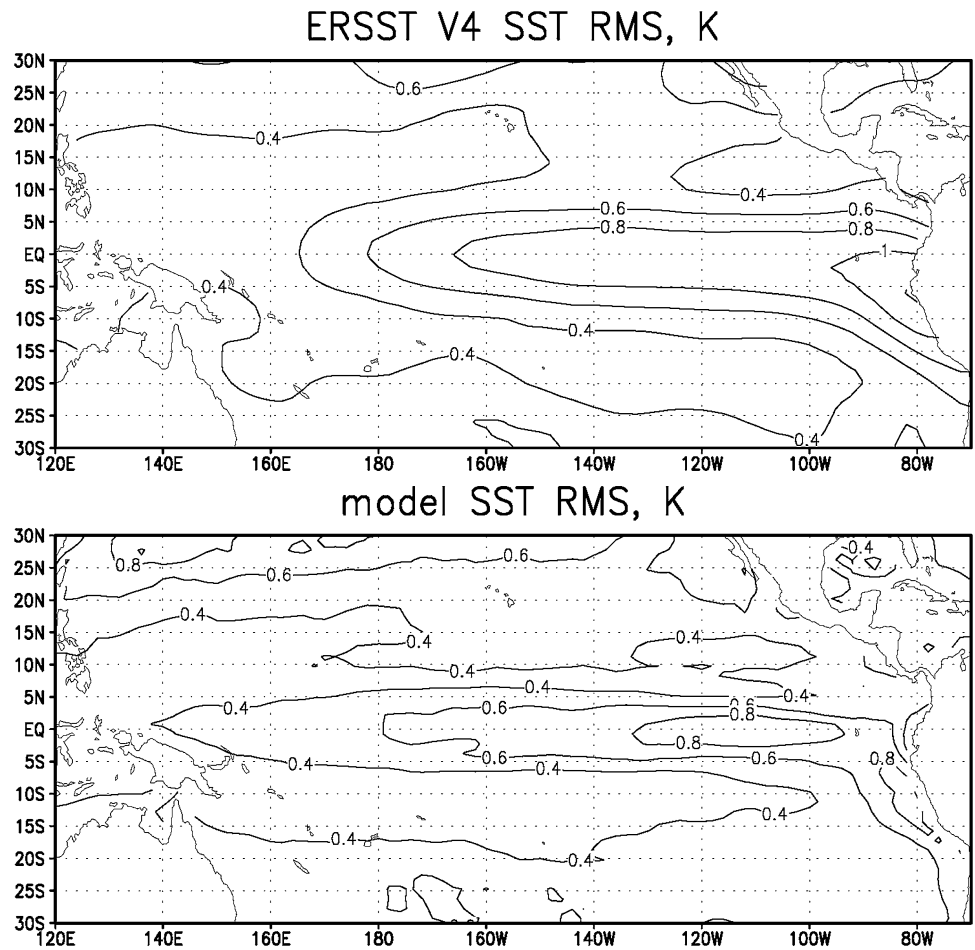


Fig. 16 Time spectrum of the sea surface temperature (K) in Nino 3, 4 region for 1865–2014 in the model (red) and ERSSTv4 (black)

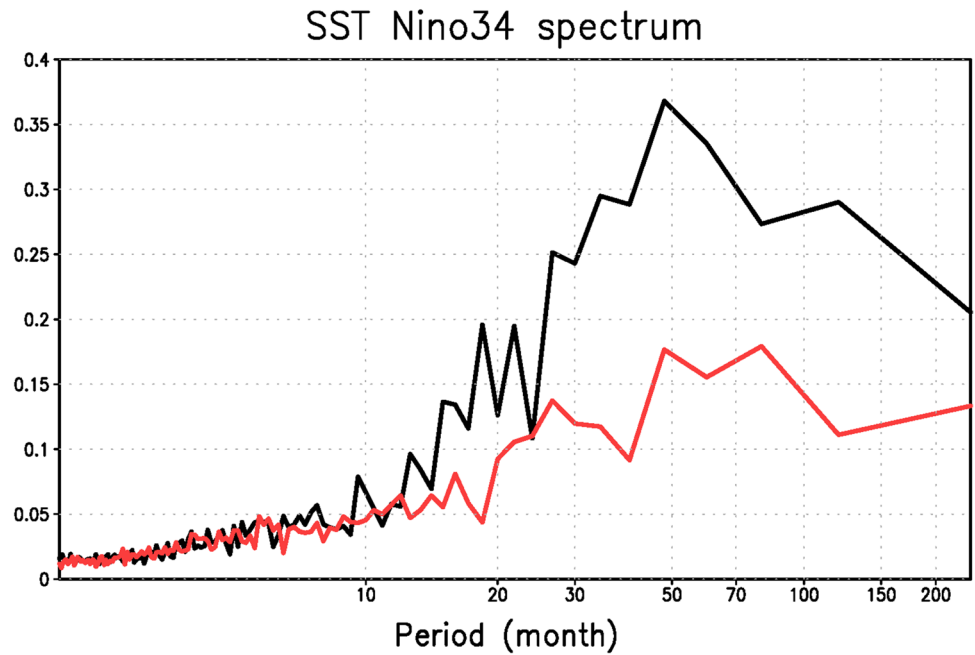
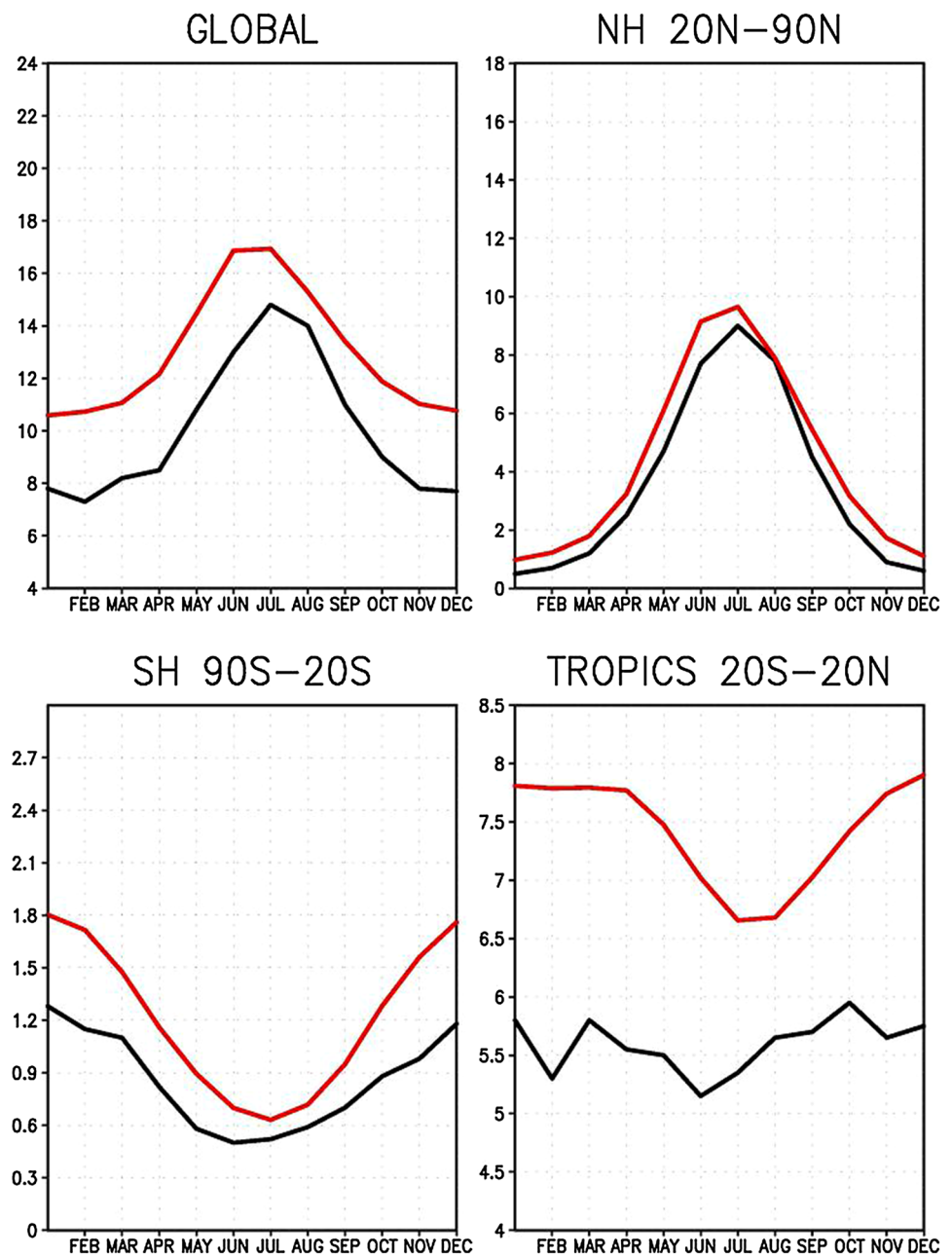


Fig. 17 Annual cycle of GPP (GtC/month) for global domain (top, left), Northern hemisphere 20N–90N (top, right), Southern Hemisphere 90S–20S (bottom, left) and tropics 20S–20N (bottom, right) in the model (red) and Stephens et al. (2007) (black) for 1986–2005



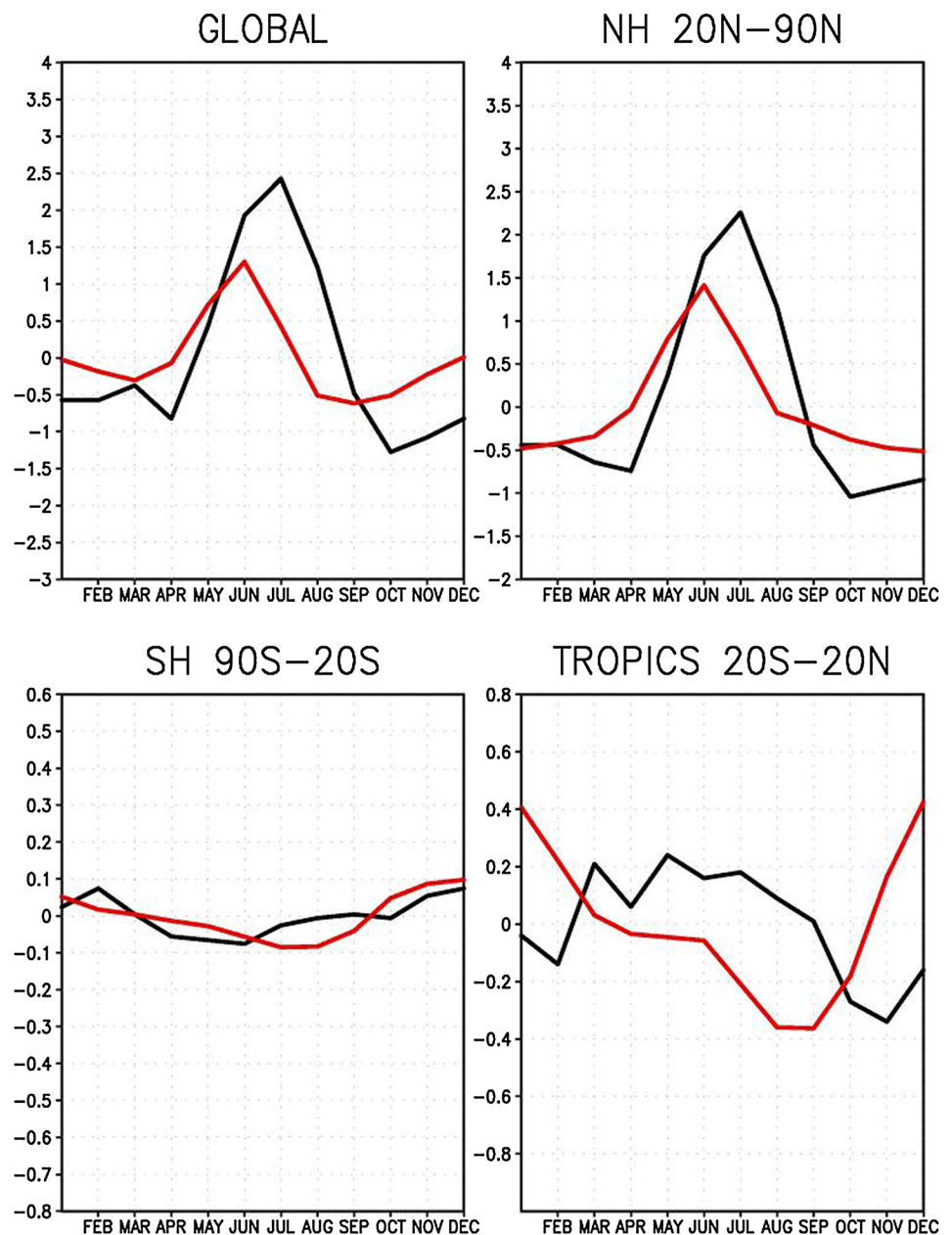
with respect to its previous version, the INMCM4. The model is capable of reproducing equatorial stratospheric QBO and SSWs.

The model biases for the sea surface height and surface salinity are reduced in the new version as well, probably due to increasing spatial resolution in the oceanic block. Bias in ocean potential temperature at depths below 700 m in the INMCM5 is also reduced with respect to the one in the INMCM4. This is likely because of the tuning background vertical diffusion coefficient. Model sea ice area is

reproduced well enough in the Arctic, but is underestimated in the Antarctic (as a result of the overestimated surface temperature). RMS error in the surface salinity is reduced almost everywhere compared to the previous model except the Arctic (where the positive bias becomes larger).

As a final remark one can conclude that the INMCM5 is substantially better in almost all aspects than its previous version and we plan to use this model as a core component for the coming CMIP6 experiment.

Fig. 18 Annual cycle of net CO₂ flux (GtC/month) for global domain (*top, left*), Northern hemisphere 20N–90N (*top, right*), Southern Hemisphere 90S–20S (*bottom, left*) and tropics 20S–20N (*bottom, right*) in the model (*red*) and Stephens et al. (2007) (*black*) for 1986–2005



Acknowledgements The study was performed at the Institute of Numerical Mathematics of the Russian Academy of Sciences and supported by the Russian Science Foundation, grant 14-17-00126 (model development) and Russian Foundation for Basic Research, grant 16-55-76004 ERA.NET RUS (numerical experiments). Climate model runs were produced at the supercomputer MVS10P of the Joint Supercomputer Center of the Russian Academy of Sciences.

References

- Adler RF, Huffman GJ, Chang A, Ferraro R, Xie P, Janowiak J, Rudolf B, Schneider U, Curtis S, Bolvin D, Gruber A, Susskind J, Arkin P (2003) The Version 2 Global Precipitation Climatology Project (GPCP) Monthly Precipitation Analysis (1979–Present). *J Hydrometeorol* 4:1147–1167
- Alekseev VA, Volodin EM, Galin VYa, Dymnikov VP, Lykossov VN (1998) Simulation of present day climate with atmospheric model of INM RAS. INM Reprint, p 198, (**available by request**)
- Anav A, Friedlingstein P, Kidston M, Bopp L, Ciais P, Cox P, Jones C, Jung M, Myneni R, Zhu Z (2013) Evaluating the land and ocean components of the global carbon cycle in the CMIP5 earth system models. *J Climate* 26:6801–6843. doi:[10.1175/JCLI-D-12-00417.1](https://doi.org/10.1175/JCLI-D-12-00417.1)
- Antonov JI et al (2010) World ocean atlas 2009, Vol. 2: Salinity. [S. Levitus (eds.)]. NOAA Atlas NESDIS 69, U.S. Gov. Printing Office, Washington, D.C., pp 184
- Asselin R (1972) Frequency filter for time integrations. *Mon Wea Rev* 100:487–490

- Betts AK (1986) A new convective adjustment scheme. Part 1. Observational and theoretical basis. *Quart J Roy Met Soc* 112:677–691
- Butchart N et al (2011) Multimodel climate and variability of the stratosphere. *J Geophys Res* 116:D05102. doi:[10.1029/2010JD014995](https://doi.org/10.1029/2010JD014995)
- Dee DP et al (2011) The ERA-Interim reanalysis: configuration and performance of the data assimilation system. *Q J R Meteorol Soc* 137:553–597
- Flato G, Marotzke J, Abiodun B, Braconnot P, Chou SC, Collins W, Cox P, Driouech F, Emori S, Eyring V, Forest C, Gleckler P, Guilyardi E, Jakob C, Kattsov V, Reason C, Rummukainen M (2013) Evaluation of climate models. In: *Climate change 2013: the physical science basis. contribution of working group I to the fifth assessment report of the intergovernmental panel on climate change* [Stocker TF, Qin D, Plattner G-K, Tignor M, Allen SK, Boschung J, Nauels A, Xia Y, Bex V, Midgley PM (eds)]. Cambridge University Press, Cambridge
- Galini VYa (1998) Parametrization of radiative processes in the DNM atmospheric model. *Izv Atmos Ocean Phys* 34:339–347
- Galini VYa, Volodin EM, Smyshlyaev SP (2003) Atmospheric general circulation model with ozone dynamics. *Rus Meteorol Hydrol N5*:7–15
- Hines CO (1997) Doppler spread parameterization of gravity wave momentum deposition in the middle atmosphere 2. Broad and quasimonochromatic spectra, and implementation. *J Atm Sol Terr Phys* 59:387–400
- Huang B, Banzon VF, Freeman E, Lawrimore J, Liu W, Peterson TC, Smith TM, Thorne PW, Woodruff SD, Zhang H-M (2015) Extended reconstructed sea surface temperature version 4 (ERSST.v4): part I. upgrades and intercomparisons. *J Climate* 28:911–930
- Hurrell JW, Hack JJ, Shea D, Caron JM, Rosinski J (2008) A new sea surface temperature and sea ice boundary dataset for the community atmosphere model. *J Climate* 21:5145–5153
- Iakovlev NG (2009) Reproduction of the large scale state of water and sea ice in the Arctic Ocean in 1948–2002. Part 1. Numerical model. *Izv Atmos Ocean Phys* 45:357–371. doi:[10.1134/S0001433809030098](https://doi.org/10.1134/S0001433809030098)
- Iakovlev NG, Volodin EM, Gritsun AS (2016) Simulation of the spatiotemporal variability of the World Ocean sea surface height by the INM climate models. *Izv Atmos Ocean Phys* 52(4):376–385. doi:[10.1134/S0001433816040125](https://doi.org/10.1134/S0001433816040125)
- Jung M, Reichstein M, Bondeau A (2009) Towards global empirical upscaling of FLUXNET eddy covariance observations: validation of a model tree ensemble approach using a biosphere model. *Biogeosciences* 6:2001
- Kessler E (1969) On the distribution and continuity of water substance in atmospheric circulations. *Meteor. Monogr.* 10. N32, Amer Meteor Soc p 84
- Kulyamin DV, Volodin EM, Dymnikov VP (2009) Simulation of the quasi-biannual oscillation in the zonal wind in the equatorial stratosphere: Part II. Atmospheric general circulation models. *Izv Atmos Ocean Phys* 45:37–54
- Landerer FW, Gleckler PJ, Lee T (2014) Evaluation of CMIP5 dynamic sea surface height multi-model simulations against satellite observations. *Clim Dyn* 43:1271–1283. doi:[10.1007/s00382-013-1939-x](https://doi.org/10.1007/s00382-013-1939-x)
- Loeb NG et al (2009) Toward optimal closure of the Earth's top-of-atmosphere radiation budget. *J Climate* 22:748–766
- Mao J, Thornton P, Shi X, Zhao M, Post W (2012) Remote sensing evaluation of CLM4 GPP for the period 2000 to 2009. *J Climate* 25:5327–5342
- Mareev EA, Volodin EM (2014) Variations of the global electric circuit and the ionospheric potential in a general circulation model. *Geophys Res Lett* 41:9009–9016. doi:[10.1002/2014GL062352](https://doi.org/10.1002/2014GL062352)
- Mueller B, Seneviratne SI (2014) Systematic land climate and evapotranspiration biases in CMIP5 simulations. *Geophys Res Lett* 41:128–134. doi:[10.1002/2013GL058055](https://doi.org/10.1002/2013GL058055)
- Palmer TN, Shutts GJ, Swinbank R (1986) Alleviation of a systematic westerly bias in general circulation and numerical weather prediction models through an orographic gravity wave drag parameterization. *Quart J Roy Met Soc* 112:1001–1031
- Rio M-H, Hernandez F (2004) A mean dynamical topography computed over the world ocean from altimetry, in-situ measurements and a geoid model. *J Geophys Res* 109:C12032. doi:[10.1029/2003JC002226](https://doi.org/10.1029/2003JC002226)
- Stephens BB et al (2007) Weak northern and strong tropical land carbon uptake from vertical profiles of atmospheric CO₂. *Science* 316:1732–1735
- Taylor KE, Stouffer RJ, Meehl GA (2012) An overview of CMIP5 and the experiment design. *Bull Am Met Soc* 93:485–498
- Terekhov KM, Volodin EM, Gusev AV (2011) Methods and efficiency estimation of parallel implementation of the σ -model of general ocean circulation. *Russ J Num Anal Math Model* 26(2):189–208
- Tiedtke M (1993) Representation of clouds in large-scale models. *Mon Weather Rev* 121:3040–3061
- Todd-Brown KEO, Randerson JT, Post WM, Hoffman FM, Tarnocai C, Schuur EA, Allison SD (2012) Causes of variation in soil carbon predictions from CMIP5 Earth system models and comparison with observations. *Biogeosci Discuss* 9:14,437–14,473
- Trenberth KE, Caron JM (2001) Estimates of meridional atmosphere and ocean heat transports. *J Clim* 14:3433–3443
- Vargin PN, Volodin EM (2016) Analysis of the reproduction of dynamic processes in the stratosphere using the climate model of the Institute of Numerical Mathematics, Russian Academy of Sciences. *Izv Atmos Ocean Phys* 52:1–15
- Volodin EM (2007) Atmosphere—ocean general circulation model with carbon cycle. *Izv Atmos Ocean Phys* 43:266–280
- Volodin EM (2008) Methane cycle in the INM RAS climate model. *Izv Atmos Ocean Phys* 44:153–159
- Volodin EM (2013) The mechanism of multidecadal variability in the Arctic and North Atlantic in climate model INMCM4. *Environ Res Lett* 8:035038. doi:[10.1088/1748-9326/8/3/035038](https://doi.org/10.1088/1748-9326/8/3/035038)
- Volodin EM, Kostrykin SV (2016) The Aerosol module in the INM RAS climate model. *Rus Meteorol Hydrol* 41(8):519–528
- Volodin EM, Lykosov VN (1998) Parametrization of heat and moisture transfer in the soil-vegetation system for use in atmospheric general circulation models: 1. Formulation and simulations based on local observational data. *Izv Atmos Ocean Phys* 34:405–416
- Volodin EM, Dianskii NA, Gusev AV (2010) Simulating present day climate with the INMCM4.0 coupled model of the atmospheric and oceanic general circulations. *Izv Atmos Ocean Phys* 46:414–431
- Volodin EM, Diansky NA, Gusev AV (2013) Simulation and prediction of climate changes in the 19th to 21st centuries with the Institute of Numerical Mathematics, Russian Academy of Sciences, model of Earth climate system. *Izv Atmos Ocean Phys* 46:347–366
- Welp LR et al (2011) Interannual variability in the oxygen isotopes of atmospheric CO₂ driven by El Niño. *Nature* 477:579–582
- Zalesny VB, Marchuk GI, Agoshkov VI, Bagno AV, Gusev AV, Diansky NA, Moshonkin SN, Tamsalu R, Volodin EM (2010) Numerical simulation of large-scale ocean circulation based on the multicomponent splitting method. *Russ J Num Anal Math Model* 25(6) 581–609